Investigating Delays in Frequency-Dependent Load Control

Mahraz Amini (Student Member, IEEE) and Mads Almassalkhi (Member, IEEE)
Department of Electrical Engineering
University of Vermont, Burlington, VT 05403, USA
{mamini2,malmassa}@uvm.edu

***Abstract*— Increased penetration of renewables will require significant regulating reserves, so there is a need to re-think the traditional operating paradigm: *supply follows demand*. Recent work has expanded the role of flexible and controllable energy resources, such as energy storage and dispatchable demand, to regulate power imbalances and stabilize grid frequency. However, as shown in this paper, the large-scale deployment of dispatchable (i.e., controllable) loads needs to carefully consider the existing regulation schemes in power systems, i.e., generator droop control. That is, this paper illustrates with a standard linearized model, the complex nature of system-wide frequency stability from time-delays in actuation of dispatchable loads and the effect of different network topologies. Interestingly, we show that delay-induced instability can be stabilized by injecting additional delay into load controller.**

***Index Terms*— dynamics, load control, swing equation, frequency droop, time delay.**

I. Introduction

The quality of delivered electrical power and safety of electrical facilities are related to the nominal system frequency (e.g., 60 Hz in the U.S.). Small frequency deviations from nominal is generally caused by active power imbalances between generation and demand and is regulated through local (proportional) adjustments in the generator's governor (i.e., primary frequency control or PFC). PFC events generally take less than 30 seconds to stabilize the system frequency [1]. However, with energy policy rapidly increasing the penetration of intermittent and low-inertia renewable generation, e.g., PV solar and wind farms, frequency deviations from nominal power imbalances are increasing [2], [3], which raises concerns over the ability of PFC to operate well in a future power system with significant penetrations of renewable energy. As such, partial automated participation of flexible loads (e.g., energy storage and demand) in response to system frequency represents an alternative.

Previously, load "control" (i.e., *load shedding*) was employed when severe imbalances threatened system integrity. More recently, active consumer-side participation has led to some revision on the former demand side control logic [4]. The concept of active consumer load coordination (i.e., aggregation) of air conditioners, radiators, plug-in electrical vehicles and other home appliances to balance the supply and demand has been discussed widely as means to reduce needed power reserves [5], [6], [7]. In fact, grid-scale distributed load frequency control algorithms have been proposed for stabilizing system frequency [8], [9]. However, due to phasor measurement units' (PMUs') communication channels that transmit data to the actuators or load coordinators (i.e., an aggregator), actuators or coordinators processing the PMU data, and the physical characteristics of the actuators and aggregators, significant constant or variable time-delays can be observed in power systems[1][10]. Prior work has focused on designing generator control loops (i.e., PFC and AGC) that are robust against uncertain time-delays [11], [12], [13], but little (if any) work has considered the effect of time-delays on load coordination algorithms and system-wide effects. Therefore, to maximize the potential of fully automated load aggregation (at the MW-scale), the role

*Funding have been graciously provides by UVM faculty startup grant. Authors would like to thank Prof. Johanna Mathieu for valuable discussions.

[1]Note: the delays considered herein are assumed to include the time for actuators or coordinators to compute desired control signals from PMU data and for the underlying loads to physically provide expected change in dispatch. That is, we do not only consider the small delays in load control associated with PMU communication delays.

of time-delayed load dispatch in power networks and its interaction with PFC schemes must be fully investigated.

To this effect, we present herein preliminary results on the system-wide effects of time-delays in flexible frequency-dependent loads. Specifically, we investigate through simulation-based analysis how different transmission network structures, dispatchable scenarios, and delays affect performance and stability of load coordination schemes.

The paper is organized as follows. Section II details the dynamical system model. In Section III, the simulated test systems and performance metrics are defined. Section IV discusses simulation results and conclusions are provided on Section V.

II. Dynamic System Model

Consider a graph $\mathcal{G} = (\mathcal{V}, \mathcal{E})$ with a set of buses $\mathcal{V}$ and lines $\mathcal{E}$. Then, the balanced N-bus transmission system with E lines will have buses divided into two sets: generator buses and load buses. A bus with a generator is called a generator bus, while all other buses are called load buses (even if the load is zero).

The voltage phase angle of bus i with respect to the rotating framework at nominal frequency is denoted θ_i and let the angular frequency deviation of bus i from nominal frequency w_i^{nom} be denoted $\Delta\omega_i := \omega_i - \omega_i^{\text{nom}}$. Then, their relationship is:

$$\dot{\theta}_i(t) = \Delta\omega_i(t) \quad \forall i \in \mathcal{V} \tag{1}$$

From the swing equation, we relate changes in frequency to instantaneous power imbalances:

$$\begin{aligned} M_i\Delta\dot{\omega}_i(t) = \Delta P_i^m(t) - \Delta P_i^e(t) \\ - D_i\Delta\omega_i(t) - \Delta d_i(t) \end{aligned} \tag{2}$$

$$\Delta P_i^e(t) = \sum_{j\in\Omega_i^N} \Delta P_{ij}(t) \tag{3}$$

$$\Delta P_{ij}(t) = b_{ij}\left(\Delta\theta_i(t) - \Delta\theta_j(t)\right) \tag{4}$$

where $\Delta P_i^m, \Delta P_i^e, \Delta d_i, \Delta P_{ij}$ are the changes in injected generator mechanical power, generator electrical power output to neighboring buses of i (i.e., Ω_i^N), controllable net-load, and line flow between buses i and j from nominal steady-state. M_i is the generator inertia constant and D_i is the damping coefficient accounting for mechanical rotational losses (of generators and motors at bus i). Also, the generator's droop behavior at bus i is described by the dynamics of the turbine and governor:

$$\Delta\dot{P}_i^m(t) = \frac{1}{\tau_{T_i}}(\Delta P_i^v(t) - \Delta P_i^m(t)) \tag{5}$$

$$\Delta\dot{P}_i^v(t) = \frac{1}{\tau_{G_i}}(\Delta P_{\text{ref,i}} - \Delta P_i^v(t) - \frac{1}{r_i}\Delta\omega_i) \tag{6}$$

where ΔP_i^v is the change in turbine output power from nominal, $\Delta P_{\text{ref,i}}$ is the change in reference power of generator i, and $\tau_{T_i}, \tau_{G_i}, r_i$ are time-constants of turbine, governor, and speed-regulator, respectively.

In the case when there is no generator at bus i (i.e., i is a load bus), $M_i = 0$ and we have the following algebraic equation describing net-flow into bus i:

$$D_i\Delta\omega_i(t) = -\Delta P_i^e(t) - \Delta d_i(t), \tag{7}$$

which through differentiation can be re-written as a dynamic state:

$$D_i\Delta\dot{\omega}_i(t) = -\sum_{j\in\Omega_i^N} \Delta\dot{P}_{ij}(t) - \Delta\dot{d}_i(t). \tag{8}$$

Finally, (4) is transformed into a dynamic equation through differentiation:

$$\Delta\dot{P}_{ij}(t) = b_{ij}\left(\Delta\omega_i(t) - \Delta\omega_j(t)\right). \tag{9}$$

An overview of the system model for lines and buses is provided in Table I. The controllable inputs are $\Delta d_i, \Delta\dot{d}_i$ and represent the control of flexible energy resources such as demand and storage. That is, in addition to the governor response of the generators, the controllable loads in the system respond to the imbalances through sensed frequency deviations and is implemented with proportional ($P_i > 0$) control as follows:

$$\Delta d_i(t) = P_i\Delta\omega_i(t - t_d) \qquad \forall i \in \mathcal{V}, \tag{10}$$

where $t_d \geq 0$ is the time-delay in load response. Note that the dynamic system model described by Eqs.(1)-(10) represents a closed-loop system with generator droop and (delayed) load control reacting to changes in sensed local frequencies.

The continuous-time dynamic model is implemented in MATLAB in discrete-time via Modified Euler with sampling time $h = 0.001$s, which has (global) accuracy on the order of $\mathcal{O}(h^2)$ [14].

TABLE I: Power system model overview

Variable Type	Variables
Dynamic states	$\Delta\omega_i, \theta_i, \Delta P_i^m, \Delta P_i^v$
Control inputs	$\Delta d_i, \Delta \dot{d}_i$
Constant Parameters	$M_i, D_i, b_{ij}, \tau_{T_i}, \tau_{G_i}, r_i$

Remark II.1 *Since the delay is applied to the (measured) state in the controllable load's closed-loop description in* (10)*, the time delay is internal to the closed-loop system, which is more challenging to analyze than the case of external (input/output) delays in the open loop. For example, an internally delayed system with input disturbance* $v(t)$ *can be described by* $\dot{x} = Ax + A_d x(t - t_d) + Wv(t)$ *and* $y = Cx(t)$*. Then, the transfer matrix is given by:*

$$H(s) = \frac{Y(s)}{V(s)} = C\left(sI - A - A_d e^{-t_d s}\right)^{-1} W.$$

The poles of transfer function $[H(s)]_{ij}$ *determine stability of output* i *with respect to disturbance* j*.*

III. Simulation Setup

In this section, we describe the different N-bus networks and the controllable load delay scenarios to be investigated.

A. Test networks

We consider three small 4-bus networks (see Fig. 1) with different interconnections (e.g., radial and meshed) and two standard IEEE test cases: 9-bus and 30-bus systems. Network parameters for the 4-bus system are based on [15] and provided in Table II. For simplicity, a generator and load is connected to each bus. Note that controllable loads provide regulation at the scale of the damping coefficients, which is an order of magnitude smaller than generator inertias.

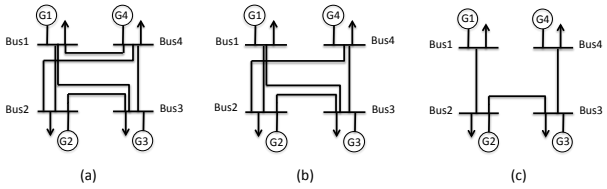

Fig. 1: Three different 4-bus networks.

TABLE II: Parameters for 4-bus system

Parameter	Value	Unit
M_1, M_2, M_3, M_4	$4, 40, 35, 10$	$\frac{pu-s^2}{rads}$
D_1, D_2, D_3, D_4	$3.7, 1, 2, 2.7$	$\frac{pu-s}{rads}$
$\tau_{T_1}, \tau_{T_2}, \tau_{T_3}, \tau_{T_4}$	5,10,20,10	s
$\tau_{G_1}, \tau_{G_2}, \tau_{G_3}, \tau_{G_4}$	4,25,15,10	s
r_1, r_2, r_3, r_4	10,15,10,12	$\frac{rads}{pu-s}$
$b_{12,13,14,23,24,34}$	$2.5, 2, 2, 1.5, 2.5, 2$	pu
$P_{i=4}$,$P_{i\neq 4}$	$3, 0$	$\frac{pu-s}{rads}$

B. Determining baseline controller gain

Before investigating the effect of time-delays, we need to design the nominal load controller's gain, P_i. The design of stabilizing P-controllers is achieved via closed-loop eigenvalue analysis of the multi-input/multi-output dynamical system and proportional gains are provided in Table II. For example, the sets of closed-loop eigenvalues of the network 1(a) is illustrated in Fig. 2 for $P_4 \in [1, 100]$. Clearly, for all P_4, the poles are stable in the left-hand plane.

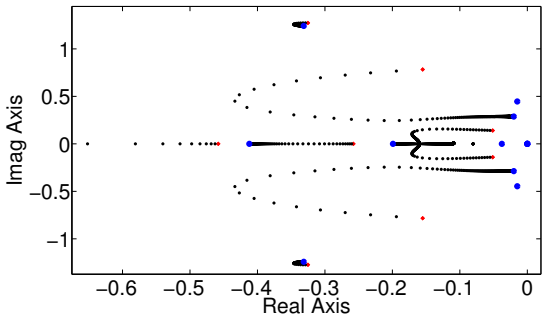

Fig. 2: Closed-loop poles for network 1a as a function of P_4. Red dot denotes $P_4 = 1$ and blue dot represents $P_4 = 100$.

C. Time-delay

Since we are interested in the interaction between delays in load control and generator governors, we limit delays to $t_d \leq 30$s. Delay t_d is then applied to the frequency-responsive load at bus $i = 4$ for the 4-bus system, buses $i = 8, 9$ for the 9-bus system, while five loads are automatically controlled (but subjected to identical delays) in the 30-bus system: buses $i = 26 - 30$.

IV. Simulation Results & Analysis

This section illustrates the non-periodic behavior of system stability for increasing delays and the effects of network structure on this stability. Interestingly, we show that delay-induced instability can be re-stabilized by injecting *additional delay* into load controller. The networks described in the previous section are initially in nominal steady-state until a +0.1 pu step-disturbance in the load at bus 1 occurs at $t = 10$ seconds.

For each applied delay t_d, the simulations capture performance (and stability conditions) through the settling time $T_{s,i}$ of the nodal frequency at bus i ($\Delta\omega_i$) and is defined as the time after which the frequency enters and remains within specified deadband, ϵ:

$$T_{s,i} = \min_t \{|\Delta\omega_i(t^*)| < \epsilon,\ \forall t^* \geq t\}.$$

Due to the finite nature of computing, we limit simulations to consider $T_{s,i} \leq 1000$ seconds. That is, the closed-loop response is unstable if $T_{s,i} = 1000s$ for any i (even if $T_{s,i}$ does not exist) and stable if $T_{s,i} < 1000s$.

A. The small 4-bus systems

The 4-bus systems in Fig. 1 are simulated according to the setup description. Note that for each t_d, we get data pair (t_d, $T_{s,i}$). Figure 3a illustrates all pairs (t_d, $T_{s,i}$) for network 1a.

Clearly, when $t_d < 2$s, the system is stable and the system frequency settles in less than 15 s. However, by increasing t_d at bus 4, the closed-loop system becomes unstable (e.g., see Fig. 4a for $t_d = 5$s) but then additional delay actually recovers stability and further delay again beget instability, etc. These stable-unstable-stable patterns repeat periodically as the load controller delay increases (e.g., see Fig. 4b for $t_d = 17 > 5$s). To validate the numerical simulations, a 10th-order Padé approximation is applied to the internal delay $e^{t_d s}$ and the resulting poles are computed from the closed-loop transfer function $\Delta\omega_2(s)/d_1(s)$ for each $t_d \leq 25$. The real part of the (complex conjugate) pole-pair traces is illustrated in Fig. 5 and confirms the stable/unstable/stable behaviors observed in numerical simulations. For each time delay t_d, the poles of the transfer function are given by a vertical slice over all traces. Note

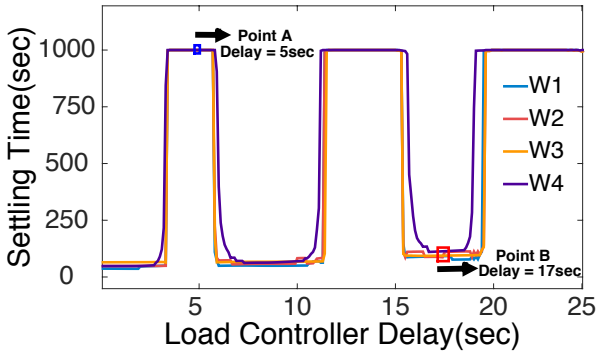

(a) Network 1a: effects of t_d at bus 4 on stability. System is initially stable ($t_d < 2$s). At Point A ($t_{d,A}$) the system is unstable, yet stable again at Point B, where: $t_{d,B} = 17s > t_{d,A} = 5s$.

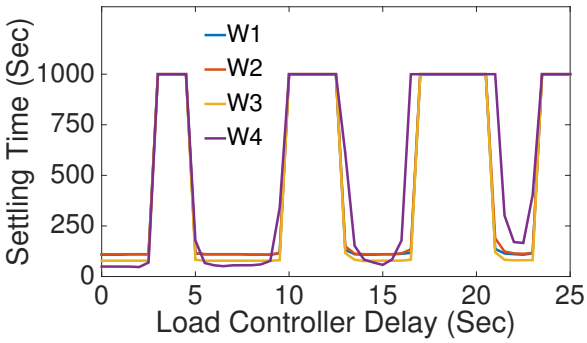

(b) Network 1b: effects of t_d at bus 4 on stability.

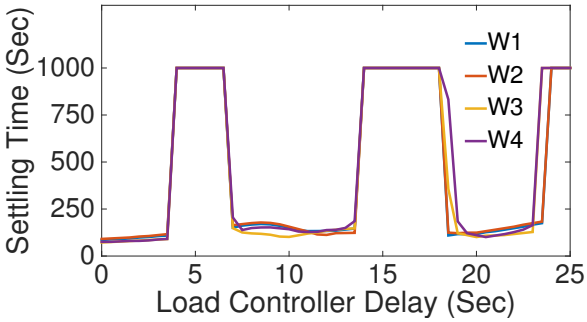

(c) Network 1c: effects of t_d at bus 4 on stability.

Fig. 3: Closed-loop system behaviors of the 4-bus system under different network configurations.

that generally $T_{s,i}$ increases with t_d. $T_{s,4}$ is most sensitive to t_d due to load controller on bus 4.

Figures 3b and 3c illustrate all pairs (t_d, $T_{s,i}$) for networks 1b and 1c. As can be seen, the performance of the 4-bus system under delays depends on the interconnection of buses. For example, pairs $(10, T_{s,i})$ illustrate this the across 4-bus networks. Thus, the 4-bus system, while simple to describe, shows the complex manner in which closed-loop

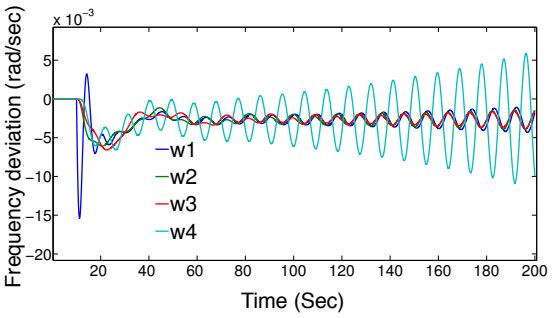

(a) Closed-loop response: Point A in Fig. 3a: $t_d = 5$s.

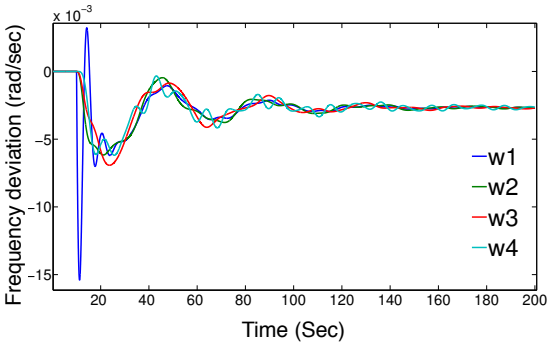

(b) Closed-loop response: Point B in Fig. 3a: $t_d = 17$s.

Fig. 4: Closed-loop and frequency responses for point A in Fig. 3a: $t_d = 5$s.

stability and instability depends on the nature of delay in actuation of frequency sensitive loads. In the next section, we investigate larger systems, which are shown to exhibit the same type of behavior.

B. The larger 9-bus and 30-bus systems

In this section, the analysis is extended to the 9-bus and 30-bus IEEE standard test cases and considers more than one controllable load to contrast with the results of the simple 4-bus networks. The settling time of the *system* is now defined as the maximum settling time across the N buses:

$$T_s := \max_i \{T_{s,i}\}$$

The IEEE 9-bus test case is simulated with load controllers at bus 8 and bus 9:

$$\Delta d_i(t) = P_i \Delta\omega_i(t - t_d) \qquad \forall i \in \{8, 9\}$$

Figure 6 illustrates all pairs of (t_d, T_s) for IEEE 9-bus test case. For $T_s < 1000s$ the system is stable while the system is unstable when $T_s = 1000s$. The stable-unstable behaviors illustrated in the 4-bus system occur also in the 9-bus case. That is,

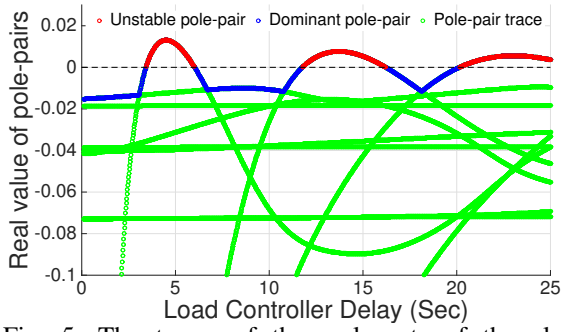

Fig. 5: The traces of the real parts of the closed-loop (complex conjugate) pole-pairs for increasing time-delays in Fig. 1a are approximated with a 10th order Padé approximation. When any pole has positive real part, the system is unstable (in red), which confirms the numerical simulation results from Fig. 3a. Note that for any given t_d, the dominant pole-pair is the trace with the largest real part and is highlighted in blue.

with increasing delay on the load controller, the settling time increases.

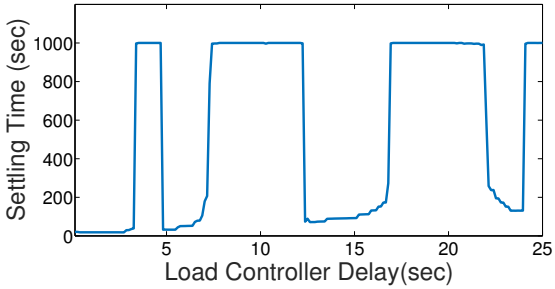

Fig. 6: Effects of t_d for controllable loads at buses 8 and 9 on closed-loop stability of 9-bus test case.

For the 30-bus network, two load control scenarios are investigated:

(i) a single controllable load at bus 30.
(ii) five controllable loads at buses $\{26 - 30\}$.

Figure 7 shows all pairs of (t_d, T_s) for the IEEE 30-bus test system under scenarios (i) and (ii). The stable-unstable behavior is also present in the closed-loop but depends on how many loads are controlled.

Remark IV.1 *As the delay increases, the periods of instability become longer, until a delay, t_d^*, is reached beyond which the system remains unstable for all $t_d > t_d^*$ and the periods of stability exhibit increasing settling times (i.e., the dominant*

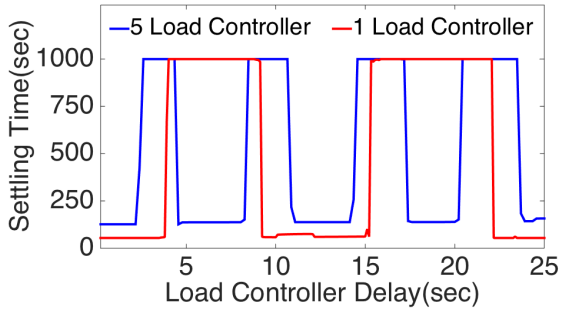

Fig. 7: The 30-bus system experiences the same stable/unstable/stable patterns for different delayed load control scenarios.

poles move closer to imaginary axis as shown in Fig. 5. Furthermore, the stable/unstable/stable patterns illustrated in this paper are expunged if the generators do not utilize droop control. This indicates that the underlying behaviors are a result of generator and load controllers fighting against each other. Ongoing work is focusing on analytically characterizing this conflict and developing an improved load control scheme.

V. Conclusion and Future Direction

This paper presents preliminary results on the effects of delay in frequency-dependent load control schemes with droop-controlled generators and investigates how delays affects settling time and stability of the system frequency in transmission networks. It is shown that the closed-loop performance of the system is stable/unstable as delay increases. Specifically, we show that the patterns of stable/unstable/stable depends on the network topology and parameters.

Future work will focus on developing analytical expressions for stability and controllability of system frequency as a function of available energy resources and salient network properties. To accomplish this, we seek to leverage recent results from linear delay differential equations where the *Lambert W function* has been utilized in describing stability of linear delay differential equations [16]. Designing controllers that are aware of actuator saturation is also being pursued. The end-goal is to develop load coordination schemes that are robust against a broad class of uncertainties, including unknown time-delays.

References

[1] A. K. Bejestani, A. Annaswamy, and T. Samad, "A hierarchical transactive control architecture for renewables integration in smart grids: Analytical modeling and stability," *IEEE Transactions on Smart Grid*, vol. 5, pp. 2054–2065, 2014.

[2] N. Miller, M. Shao *et al.*, "Eastern frequency response study," *Contract*, vol. 303, pp. 275–3000, 2013.

[3] P. Sorensen, N. A. Cutululis *et al.*, "Power Fluctuations From Large Wind Farms," *IEEE Transactions on Power Systems*, vol. 22, no. 3, pp. 958–965, 2007.

[4] D. Callaway and I. Hiskens, "Achieving Controllability of Electric Loads," *Proceedings of the IEEE*, vol. 99, no. 1, pp. 184–199, 2011.

[5] F. C. Schweppe, R. D. Tabors *et al.*, "Homeostatic utility control," *Power Apparatus and Systems, IEEE Transactions on*, no. 3, pp. 1151–1163, 1980.

[6] J. H. Eto, J. Nelson-Hoffman *et al.*, "Demand response spinning reserve demonstration," *Lawrence Berkeley National Laboratory*, 2007.

[7] A. Molina-García, F. Bouffard, and D. S. Kirschen, "Decentralized demand-side contribution to primary frequency control," *IEEE Transactions on Power Systems*, vol. 26, no. 1, pp. 411–419, 2011.

[8] C. Zhao, U. Topcu *et al.*, "Design and Stability of Load-Side Primary Frequency Control in Power Systems," *IEEE Transactions on Automatic Control*, vol. 59, no. 5, pp. 1177–1189, 2014.

[9] C. Zhao, E. Mallada, and F. Dörfler, "Distributed frequency control for stability and economic dispatch in power networks," in *Proceedings of IEEE American Control Conference*, 2015.

[10] S. Wang, X. Meng, and T. Chen, "Wide-area control of power systems through delayed network communication," *IEEE Transactions on Control Systems Technology*, vol. 20, no. 2, pp. 495–503, 2012.

[11] L. Jiang, W. Yao *et al.*, "Delay-dependent stability for load frequency control with constant and time-varying delays," *IEEE Transactions on Power Systems*, vol. 27, no. 2, pp. 932–941, 2012.

[12] C. K. Zhang, L. Jiang *et al.*, "Further results on delay-dependent stability of multi-area load frequency control," *IEEE Transactions on Power Systems*, vol. 28, no. 4, pp. 4465–4474, 2013.

[13] K. Ramakrishnan and G. Ray, "Stability Criteria for Nonlinearly Perturbed Load Frequency Systems With Time-Delay," *IEEE Journal on Emerging and Selected Topics in Circuits and Systems*, vol. 5, no. 3, pp. 383–392, 2015.

[14] T. I. Lakoba, "Lecture notes in numerical differential equations higher-order odes and systems of odes," May 2016.

[15] R. M. Hermans, A. Jokić *et al.*, "Assessment of non-centralised model predictive control techniques for electrical power networks," *International Journal of Control*, vol. 85, no. 8, pp. 1162–1177, Aug. 2012.

[16] S. Yi, P. Nelson, and A. Ulsoy, "Survey on analysis of time delayed systems via the Lambert W function," *Advances in Dynamical Systems*, vol. 14, pp. 296–301, 2007.